

Flat bands and perfect metal in trilayer moiré graphene

Christophe Mora,¹ Nicolas Regnault,¹ and B. Andrei Bernevig²

¹*Laboratoire de Physique de l'Ecole normale supérieure,
ENS, Université PSL, CNRS, Sorbonne Université,*

Université Paris-Diderot, Sorbonne Paris Cité, Paris, France

²*Department of Physics, Princeton University, Princeton, New Jersey 08544, USA*

(Dated: January 18, 2019)

We investigate the electronic structure of a twisted multilayer graphene system forming a moiré pattern. We consider small twist angles separating the graphene sheets and develop a low-energy theory to describe the coupling of Dirac Bloch states close to the K point in each individual plane. Extending beyond the bilayer case, we show that, when the ratio of the consecutive twist angles is rational, a periodicity emerges in quasimomentum space with moiré Bloch bands even when the system does not exhibit a crystalline lattice structure in real space. For a trilayer geometry, we find flat bands in the spectrum at certain rotation angles. Performing a symmetry analysis of the band model for the trilayer, we prove that the system is a perfect metal in the sense that it is gapless at all energies. This striking result originates from the three Dirac cones which can only gap in pairs and produce bands with an infinite connectivity. The full gapless property is protected by an emergent particle-hole symmetry valid at sufficiently small angles.

Two parallel layers of graphene twisted by a small angle exhibit a moiré pattern [1], with a lattice periodicity much larger than the graphene unit cell, and non-trivial electronic properties [2], such as band-flattening at certain *magic* angles [3–8]. Flat bands present a reduced kinetic energy, thereby artificially boosting electron correlations [9]. The recent discovery of correlated insulating phases at half-filling and possibly unconventional superconductivity [10–13] have unveiled bilayer moiré graphene as a tunable device for exploring novel correlated states, at zero or finite magnetic field, spurring intense theoretical work in this direction [14–33]. On the other hand, moiré bands were also investigated for their topological properties [34–40] and topological phase transitions were identified close to the magic angles [37, 41].

In view of the great wealth of correlation and topological phenomena occurring with moiré bilayer graphene, it is desirable to extend studies to multilayer, and specifically trilayer geometries, in which moiré patterns also appear for small rotation angles. Flat bands in bilayer result from an interplay between the K (or K') Dirac points in each layer and the situation with three or more Dirac points has yet to be explored. At low energy and close to half-filling, the band structure is formed only from the electron states of the Dirac cones in each layer [42]. A moiré band theory describing such a state, that does not require a crystalline lattice, is built in Ref. [3]. In this paper, we extend this theory to multilayer graphene and discuss in depth the symmetry and topology for three layers. We find magic angles of vanishing Dirac velocities; they are not related to a complete flattening of the spectrum, rather by a flattening along certain symmetry lines. We also characterize the different moiré bands by the irreducible representations they generate at the high-symmetry points and lines. Based on the compatibility between these representations [43, 44], we are able

to prove the remarkable result that all bands are connected such that no subset of bands can be energetically isolated from the others. The most obvious consequence is that the system remains metallic at arbitrary energy. This property requires particle-hole symmetry - neglecting the band curvature in the vicinity of the original K points.

Bloch band coupling. We detail the derivation of the band structure of the moiré pattern in twisted multilayer graphene. When the twisting angle is small, a moiré pattern is formed by the interference of lattices between the different layers. Restricting the analysis to Dirac fields near the K points of each layer [3, 7, 42] (see also Ref. [45]) and assuming a local short-range tunnel amplitude between atoms in consecutive planes, one derives the following Hamiltonian

$$H^{(ab)}(\delta\mathbf{p}_a, \delta\mathbf{p}_b) = v_F \delta\mathbf{p} \cdot \boldsymbol{\sigma} \delta_{a,b} + w^{ab} \sum_{j=1}^3 \delta_{\delta\mathbf{p}_a, \delta\mathbf{p}_b + \mathbf{q}_j^{a,b}} T^j \quad (1)$$

where w^{ab} are hopping energies between the neighboring layers a and b . The first term in Eq. (1) represents the Dirac cones in each layer and $\delta\mathbf{p}$ is a small momentum deviation from the K point for the layer a . We have introduced the matrices

$$T^{j+1} = \sigma_0 + \cos(2\pi j/3) \sigma_x + \sin(2\pi j/3) \sigma_y \quad (2)$$

associated with the three symmetric momentum directions $\mathbf{q}_1^{a,b} = M_{ab}\mathbf{K} - \mathbf{K}$, $\mathbf{q}_2^{a,b} = C_{3z}\mathbf{q}_1^{a,b}$, $\mathbf{q}_3^{a,b} = C_{3z}\mathbf{q}_2^{a,b}$. M_{ab} the rotation around z with the twist angle θ_{ab} separating the layers a and b and C_{3z} with angle $2\pi/3$. For small twist angles, $\mathbf{q}_1^{a,b}$ is perpendicular to \mathbf{K} so that all the $\mathbf{q}_j^{a,b}$ are parallel for fixed j (see below).

The magnitudes of the vectors $|\mathbf{q}_j^{a,b}| = 2|\mathbf{K}| \sin(\theta_{ab}/2)$ depend on the twist angles. The second term in Eq. (1)

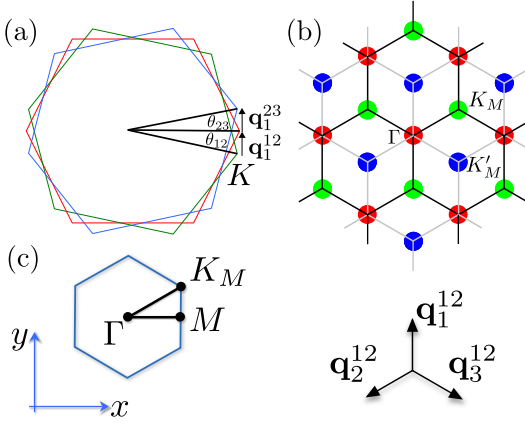


FIG. 1. Trilayer graphene with the same rotation angle $\theta_{12} = \theta_{23}$ between consecutive layers. (a) Original Brillouin zones in each layer with their respective K points. (b) k-space lattice generated by the vectors \mathbf{q}_j^{ab} (for $\mathbf{q}_j^{12} = \mathbf{q}_j^{23}$). Green, red and blue sites belong respectively to the layers 1, 2, 3. (c) Moiré Brillouin zone with high-symmetry points Γ , K_M , K'_M , M and high-symmetry lines (in black).

couples momenta $\delta\mathbf{p}_a$ and $\delta\mathbf{p}_b + \mathbf{q}_j^{a,b}$ in layers a and b which generates a lattice in momentum space for each pair of consecutive layers. To make the calculation tractable and maintain an emergent periodicity in momentum space regardless of whether the multilayer system itself is crystalline, one has to assume that the ratios of twist angles are rational numbers. This periodicity results in moiré bands which we compute numerically and classify according to their irreducible representations at the high-symmetry points and lines. On the contrary, if the twist angles were incommensurate, or the \mathbf{q}_j^{ab} vectors are not parallel for fixed j , then successive applications of the Hamiltonian (1) would reach arbitrary momentum and the moiré periodicity would be absent.

The Hamiltonian (1) reduces to the model of Ref. [3] for bilayer and we henceforth focus on the trilayer geometry. We take the rotation angle θ_{12} as a reference and introduce the moiré magnitude $k_D = 2|\mathbf{K}|\sin(\theta_{12}/2)$. We rescale all momenta by k_D and the Hamiltonian as $\tilde{H} = H/(v_F k_D)$. Fixing the direction of $\mathbf{q}_1^{a,b}$ along y , we use the complex notation

$$q_1^{23} = e^{i\frac{\pi}{2}}; \quad q_2^{23} = e^{i\frac{7\pi}{6}}; \quad q_3^{23} = e^{-i\frac{\pi}{6}}; \quad (3)$$

and $q_j^{12} = (p/q)q_j^{23}$ for all j , where p and q are coprime integers. The Hamiltonian (1) can then be written as

$$\tilde{H}_{Q_m Q_n}(k) = (\mathbf{k} - \mathbf{Q}_m) \cdot \boldsymbol{\sigma} \delta_{mn} + \alpha \sum_j T^j \delta_{Q_m, Q_n - q_j^{mn}} \quad (4)$$

where we assume a uniform tunnel amplitude $w_{ab} = w$ and introduce the dimensionless coupling $\alpha = w/(v_F k_D)$ between Dirac cones. The vectors \mathbf{Q}_m form a k -space lattice, see Fig. 1b, where each site is associated to a specific layer.

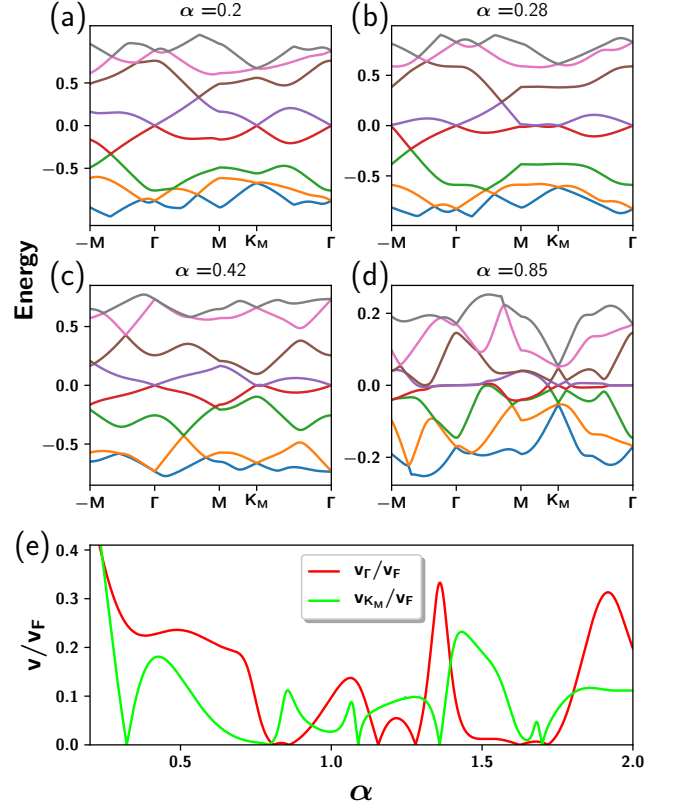


FIG. 2. Moiré bands (a-d) and renormalized Dirac-point velocities (e) at the symmetric points Γ (red) and K_M (green). The eight bands closest to zero energy are represented along the moiré Brillouin zone trajectory $-M \rightarrow \Gamma \rightarrow M \rightarrow K_M \rightarrow \Gamma$ for $\alpha = 0.2, 0.28, 0.42, 0.85$ (a-d). The particle-hole symmetry discussed in the main text - sending k to $-k$ and E to $-E$ is clearly visible along the path $-M \rightarrow \Gamma \rightarrow M$. (e) Velocities of the two Dirac cones at Γ and K_M as function of α .

Equal twist angles. We first consider the most symmetric case of evenly rotated planes where $q_j^{12} = q_j^{23}$. A representative set of moiré spectra obtained from Eq. (4) with different values of the coupling α is displayed in Fig. 2a-d. The moiré bands exhibit a rich structure. The first remarkable feature is that all bands are connected: it is impossible to isolate a set of bands which are detached from the rest. We provide below a formal proof for this statement based on irreducible representations at symmetric points and lines, and afterwards extend it to arbitrary p and q .

Three Dirac cones are attached at zero energy to the points Γ , K_M and K'_M (see Fig. 1b) as α is varied. We display the corresponding Dirac velocities of the cones at Γ and K_M (with K'_M velocity linked by symmetry to that of K_M) in Fig. 2e and find a set of *magic angles* - in analogy with the bilayer case - where one of these velocities vanishes. The difference with the bilayer case is that these magic angles are not associated with a flat-

tening of the whole spectrum which would be at odds with the fully connected band structure. However, we do see a flattening of part of the spectrum close to magic angles: on the $M - K_M$ line (for the second levels) when $\alpha = 0.28$, close to Γ when $\alpha = 0.85$, for the first two magic angles. This flattening along one-dimensional directions in k -space open interesting perspectives for the realization of exotic correlated many-body physics.

Symmetries The moiré reciprocal lattice vectors $b_1 = q_1^{12} - q_2^{12}$, $b_2 = q_1^{12} - q_3^{12}$ generate the whole lattice in Fig. 1b. The different layers (colors) are coupled by the $q_j^{a,b}$ vectors. Bloch periodicity takes the form

$$\tilde{H}(k - b_i) = V^{b_i} \tilde{H}(k) V^{b_i \dagger}, \quad V_{Q_m, Q_n}^{b_i} = \delta_{Q_n, Q_m + b_i}. \quad (5)$$

The spectrum is thus invariant upon shifting the origin of k by a combination of b_1 and b_2 .

The moiré lattice also transforms into itself by the action of a $2\pi/3$ rotation C_{3z} around Γ . In the Hamiltonian language, the corresponding operator is given by $C_{3z} = \exp(i2\pi\sigma_z/3)\delta_{Q_m, C_{3z}Q_n}$. We note that if Q_n is in a given layer so is $C_{3z}Q_n$, such that the three layers are not mixed by the rotation. The C_{2x} symmetry operates a reflexion across the x-axis going through the Γ point (red in Fig. 1b). As such, C_{2x} sends lattice sites of layer 1 to 3 and viceversa but keeps layer 2 invariant. The corresponding symmetry operator is $C_{2x} = \sigma_x \delta_{Q_m, C_{2x}Q_n}$. The two symmetry operators induce the Hamiltonian transformation

$$C_{3z} \tilde{H}(k) C_{3z}^\dagger = \tilde{H}(C_{3z}k), \quad C_{2x} \tilde{H}(k) C_{2x}^\dagger = \tilde{H}(C_{2x}k), \quad (6)$$

which leave the spectrum invariant. The antiunitary $C_{2z}\mathcal{T}$ symmetry acts locally on the moiré lattice. It takes complex conjugation K and reverses the pseudo-spin direction. It is represented by the operator $C_{2z}\mathcal{T} = \sigma_x \delta_{Q_m, Q_n} K$, which squares to 1 and commutes with the Hamiltonian $\tilde{H}(k)$. It also commutes with the spatial symmetries C_{3z} and C_{2x} .

The moiré model also possesses a unitary particle-hole (p-h) symmetry. The original $k \cdot p$ Dirac Hamiltonian of the single layer graphene sheet $H(k) = \vec{k} \cdot \vec{\sigma}$ has a unitary particle-hole symmetry $H(k) = -H(-k)$ due to the absence of k^2 terms in the Hamiltonian. Since our model is based on this low-energy expansion, it retains a similar symmetry with the operator

$$\mathcal{P} = \delta_{Q_m, -Q_n} \zeta_{Q_n} \quad (7)$$

where ζ_{Q_n} is +1 for Q_n belonging to the lower and top layers and -1 for the middle layer. With this, we have $\mathcal{P}^2 = \mathcal{P}\mathcal{P}^\dagger = 1$. Importantly, one checks that \mathcal{P} commutes with all other symmetry operators, C_{3z} , C_{2x} and $C_{2z}\mathcal{T}$, and satisfies

$$\mathcal{P} \tilde{H}(k) \mathcal{P}^\dagger = -\tilde{H}(-k). \quad (8)$$

Γ_1	Γ_2	Γ_3	M_1	M_2	K_1	$K_2 K_3$	ΓM_1	ΓM_2	
E	1	1	2	E	1	1	E	1	1
$2C_3$	1	1	-1	C_2	1	-1	C_3	1	-1
$3C_2$	1	-1	0			C_3^{-1}	1	-1	

TABLE I. Character table of irreducible representations at high symmetry momenta and lines in magnetic space group $P6'2'2$. E , C_3 , and C_2 represent the conjugation classes generated from identity, C_{3z} and C_{2x} . The notation ΓM_i stands for the symmetric line $\Gamma - M$.

This is to be contrasted with the p-h operator \mathcal{P}_{bi} identified [37] for moiré bilayer which has: (i) $\mathcal{P}_{bi}^2 = 1$, and (ii) anticommutes with C_{2x} , *i.e.* $\{\mathcal{P}_{bi}, C_{2x}\} = 0$, instead of the commutation found for \mathcal{P} .

Based on the generators discussed so far, the symmetry group of the moiré lattice is the magnetic space group called $P6'2'2$ (#177.151 in the BNS notation [46]). Although the same group describes moiré bilayer, the physics is different here. It indeed originates from 3 Dirac cones, instead of two, and the extra particle-hole symmetry is essentially different. The high-symmetry points and their little co-groups are Γ ($C_{2x}, C_{3z}, C_{2z}\mathcal{T}, \mathcal{P}$), K_M ($C_{3z}, C_{2z}\mathcal{T}, \mathcal{P}C_{2x}$) and M ($C_{2x}, C_{2z}\mathcal{T}, \mathcal{P}$). The symmetries on the high-symmetry lines are $\Gamma - M$ ($C_{2x}, C_{2z}\mathcal{T}$) and $\Gamma - K_M$ ($C_{2x}\mathcal{P}, C_{2z}\mathcal{T}$). The classification of the different irreducible representations at the symmetric points and lines are given in Table I. At Γ , M , K_M and on the line $\Gamma - M$, each energy or band in Fig. 2 is characterized by a certain representation determined from the character, *i.e.* from the eigenvalues of the operators C_{3z} and C_{2x} restricted to this (possibly degenerate) energy.

First proof of all-connected bands. We now prove by contradiction that all bands are connected such that there is no gap in the spectrum at any energy. We assume a subspace of isolated bands between the energies $\varepsilon_{1,k}$ and $\varepsilon_{2,k}$. By p-h symmetry, a symmetric set of bands exists in the energy window $(-\varepsilon_{2,-k}, -\varepsilon_{1,-k})$ and, consequently, the N_1 bands between $-\varepsilon_{1,-k}$ and $\varepsilon_{1,k}$ must be disconnected from all other bands. We focus on these N_1 bands and investigate their transformation property under C_{2x} . C_{2x} remains a symmetry along the line connecting Γ and M such that their total character must coincide at each end, or $\chi_{C_2\Gamma} = \chi_{C_2M}$.

We call m_{Γ_i} the multiplicity of the representation $i = 1, 2, 3$ in the set of N_1 bands, and m_{M_i} the multiplicity of the representation $i = 1, 2$ in the set of N_1 bands at M . Hence we have the equations: $m_{\Gamma_1} + m_{\Gamma_2} + 2m_{\Gamma_3} = N_1$, $m_{M_1} + m_{M_2} = N_1$, $m_{\Gamma_1} - m_{\Gamma_2} = \chi_{C_2\Gamma}$ and $m_{M_1} - m_{M_2} = \chi_{C_2M}$ which leads to

$$m_{M_2} = m_{\Gamma_2} + m_{\Gamma_3}. \quad (9)$$

For $\alpha = 0$, we have three Dirac cones around Γ , K_M and K'_M and a gapped spectrum at M . At Γ , the zero energy subspace is doubly degenerate and the character of C_{3z}

is simply given by $\text{Tr}(e^{i\frac{2\pi}{3}\sigma_z}) = -1$ corresponding to the irreducible representation Γ_3 as indicated in Table I. We thus have $m_{\Gamma_3} = 1$, $m_{M_2} = m_{\Gamma_2} = 0$ when restricted to zero energy and $\alpha = 0$. Increasing α away from zero, the \mathcal{P} symmetry is maintained and commutes with \mathcal{C}_{3z} and \mathcal{C}_{2x} such that any band associated to a given representation collapsing at (or departing from) zero energy, at either Γ or M , must move with its energy symmetric p-h partner associated to the same representation. As a result, the multiplicities m_{Γ_j} and m_{M_j} can only change by units of two in such processes. The same argument extends to non-zero energies where each band with energy ε and representation Γ_j (or M_j) has a p-h partner with energy $-\varepsilon$ and the same representation. Since k and $-k$ are identified at Γ and M such that the interval $(-\varepsilon_{1,-k}, +\varepsilon_{1,k})$ is symmetric, we finally obtain by continuity with α that the multiplicity m_{Γ_3} must be odd while m_{M_2} and m_{Γ_2} are both even integers. It contradicts Eq. (9), thus completing the proof.

General proof for unequal twist angles. Our discussion was so far restricted to the symmetric configuration of equal p and q . The \mathcal{C}_{2x} and \mathcal{P} symmetries are broken when p and q are different whereas \mathcal{C}_{3z} and $\mathcal{C}_{2z}\mathcal{T}$ are maintained. However, a remnant of p-h symmetry still exists in the form of a mirror symmetry $\Pi_{\pi/6}$ with respect to the plane orthogonal to the layer and crossing Γ and K_M , leaving each layer invariant. It corresponds to the operator $\Pi_{\pi/6} = \mathcal{P}\mathcal{C}_{2x}\mathcal{C}_{3z}$ with $\Pi_{\pi/6}^2 = 1$, acting as

$$\Pi_{\pi/6}\tilde{H}(k)\Pi_{\pi/6}^\dagger = -\tilde{H}(\Pi_{\pi/6}k), \quad (10)$$

which associates pairs of mirror-symmetric momenta with opposite energies. Extending the arguments of Ref. [38], we show that a set of isolated bands with $\mathcal{C}_{2z}\mathcal{T}$ symmetry cannot accommodate an odd winding number N_t , corresponding for example to an odd number of Dirac cones. The derivation is explicit in Ref. [37, 38] for two bands and a vanishing total Berry phase (Wilson loop) with $N_t = -2e_2$, where the Euler class e_2 is an integer topological invariant. Adding more bands, windings around singularities can change sign but keep a definite parity while the parity of e_2 defines a \mathbb{Z}_2 topological invariant, the Stiefel-Whitney class w_2 . Then, the relation $N_t = -2w_2$ simply enforces that the winding number must be an even integer. More intuitively, we note that Dirac points are monopoles attaching Dirac strings. They can annihilate in pairs when of opposite signs or form a topological isolated band by combining pairs of same sign [36, 37], but in all cases they need to pair to form an isolated set of bands.

We now show by contradiction that all bands are connected by gapless points in our trilayer moiré model for arbitrary p and q . As already discussed above, we can assume, without loss of generality, a set of disconnected bands symmetric around zero energy. P-h symmetry implies that all band crossings at non-zero energy come in

pair such that the analysis of the parity of N_t can be restricted to zero-energy modes. A single Dirac cone is protected by $\mathcal{C}_{2z}\mathcal{T}$ and is pinned at zero energy by p-h sP. p-h further protects the parity of N_t for zero modes as α is varied. By continuity with the case $\alpha = 0$ where we have three Dirac cones and $N_t = 3$, we finally obtain that N_t is odd, in contradiction with $N_t = -2w_2$, which completes our proof that all bands must be connected.

In summary, we showed that trilayer twisted graphene exhibits band flattening along symmetry lines and close to magic angles. We also proved, by compatibility of band representations for evenly twisted planes or by counting an odd number of Dirac points protected by $\mathcal{C}_{2z}\mathcal{T}$, that the system is always a metal with an infinite connectivity, an unprecedented feature in standard materials [43, 47–49]. This property relies on p-h symmetry emerging for small twisting angles. We checked that this condition is practically realized already for angles close to the first magic angle [50]. Since it originates from the underlying three Dirac cones, we conjecture that the property of infinite band connectivity will appear in many other configuration such as multilayer moiré graphene with an odd number of planes.

We would like to thank B. Estienne and Biao Lian for fruitful discussions. BB is supported by the Department of Energy Grant No. de-sc0016239, the National Science Foundation EAGER Grant No. noaawd1004957, Simons Investigator Grants No. ONRN00014-14-1-0330, No. ARO MURI W911NF-12-1-0461, and No. NSF-MRSEC DMR-1420541, the Packard Foundation, the Schmidt Fund for Innovative Research.

-
- [1] Wing-Tat Pong and Colm Durkan, “A review and outlook for an anomaly of scanning tunnelling microscopy (stm): superlattices on graphite,” *Journal of Physics D: Applied Physics* **38**, R329 (2005).
 - [2] R. Bistritzer and A. H. MacDonald, “Transport between twisted graphene layers,” *Phys. Rev. B* **81**, 245412 (2010).
 - [3] Rafi Bistritzer and Allan H MacDonald, “Moiré bands in twisted double-layer graphene,” *Proceedings of the National Academy of Sciences* **108**, 12233–12237 (2011).
 - [4] G. Trambly de Laissardiere, D. Mayou, and L. Magaud, “Localization of dirac electrons in rotated graphene bilayers,” *Nano Letters* **10**, 804–808 (2010).
 - [5] P. San-Jose, J. González, and F. Guinea, “Non-abelian gauge potentials in graphene bilayers,” *Phys. Rev. Lett.* **108**, 216802 (2012).
 - [6] J. M. B. Lopes dos Santos, N. M. R. Peres, and A. H. Castro Neto, “Continuum model of the twisted graphene bilayer,” *Phys. Rev. B* **86**, 155449 (2012).
 - [7] Shiang Fang and Efthimios Kaxiras, “Electronic structure theory of weakly interacting bilayers,” *Phys. Rev. B* **93**, 235153 (2016).
 - [8] Grigory Tarnopolsky, Alex J Kruchkov, and Ashvin Vishwanath, “Origin of magic angles in twisted bilayer

- graphene,” arXiv preprint arXiv:1808.05250 (2018).
- [9] Kyoungwan Kim, Ashley DaSilva, Shengqiang Huang, Babak Fallahazad, Stefano Larentis, Takashi Taniguchi, Kenji Watanabe, Brian J. LeRoy, Allan H. MacDonald, and Emanuel Tutuc, “Tunable moiré bands and strong correlations in small-twist-angle bilayer graphene,” *Proceedings of the National Academy of Sciences* **114**, 3364–3369 (2017).
 - [10] Yuan Cao, Valla Fatemi, Ahmet Demir, Shiang Fang, Spencer L Tomarken, Jason Y Luo, Javier D Sanchez-Yamagishi, Kenji Watanabe, Takashi Taniguchi, Efthimios Kaxiras, *et al.*, “Correlated insulator behaviour at half-filling in magic-angle graphene superlattices,” *Nature* **556**, 80 (2018).
 - [11] Yuan Cao, Valla Fatemi, Shiang Fang, Kenji Watanabe, Takashi Taniguchi, Efthimios Kaxiras, and Pablo Jarillo-Herrero, “Unconventional superconductivity in magic-angle graphene superlattices,” *Nature* **556**, 43 (2018).
 - [12] Stephen Carr, Shiang Fang, Pablo Jarillo-Herrero, and Efthimios Kaxiras, “Pressure dependence of the magic twist angle in graphene superlattices,” *Phys. Rev. B* **98**, 085144 (2018).
 - [13] Matthew Yankowitz, Shaowen Chen, Hryhorii Polshyn, K Watanabe, T Taniguchi, David Graf, Andrea F Young, and Cory R Dean, “Tuning superconductivity in twisted bilayer graphene,” arXiv preprint arXiv:1808.07865 (2018).
 - [14] Noah F. Q. Yuan and Liang Fu, “Model for the metal-insulator transition in graphene superlattices and beyond,” *Phys. Rev. B* **98**, 045103 (2018).
 - [15] Fengcheng Wu, A. H. MacDonald, and Ivar Martin, “Theory of phonon-mediated superconductivity in twisted bilayer graphene,” *Phys. Rev. Lett.* **121**, 257001 (2018).
 - [16] Bikash Padhi, Chandan Setty, and Philip W. Phillips, “Doped twisted bilayer graphene near magic angles: Proximity to wigner crystallization, not mott insulation,” *Nano Letters* **18**, 6175–6180 (2018), pMID: 30185049, <https://doi.org/10.1021/acs.nanolett.8b02033>.
 - [17] Hoi Chun Po, Liujun Zou, Ashvin Vishwanath, and T. Senthil, “Origin of mott insulating behavior and superconductivity in twisted bilayer graphene,” *Phys. Rev. X* **8**, 031089 (2018).
 - [18] Hiroki Isobe, Noah F. Q. Yuan, and Liang Fu, “Unconventional superconductivity and density waves in twisted bilayer graphene,” *Phys. Rev. X* **8**, 041041 (2018).
 - [19] J. F. Dodaro, S. A. Kivelson, Y. Schattner, X. Q. Sun, and C. Wang, “Phases of a phenomenological model of twisted bilayer graphene,” *Phys. Rev. B* **98**, 075154 (2018).
 - [20] G. Baskaran, “Theory of Emergent Josephson Lattice in Neutral Twisted Bilayer Graphene (Moiré is Different),” ArXiv e-prints (2018), arXiv:1804.00627 [cond-mat.supr-con].
 - [21] T. Huang, L. Zhang, and T. Ma, “Antiferromagnetically ordered Mott insulator and $d + id$ superconductivity in twisted bilayer graphene: A quantum Monte carlo study,” ArXiv e-prints (2018), arXiv:1804.06096 [cond-mat.supr-con].
 - [22] Y.-Z. You and A. Vishwanath, “Superconductivity from Valley Fluctuations and Approximate SO(4) Symmetry in a Weak Coupling Theory of Twisted Bilayer Graphene,” ArXiv e-prints (2018), arXiv:1805.06867 [cond-mat.str-el].
 - [23] X.-C. Wu, K. A. Pawlak, C.-M. Jian, and C. Xu, “Emergent Superconductivity in the weak Mott insulator phase of bilayer Graphene Moiré Superlattice,” ArXiv e-prints (2018), arXiv:1805.06906.
 - [24] B. Roy and V. Juricic, “Unconventional superconductivity in nearly flat bands in twisted bilayer graphene,” ArXiv e-prints (2018), arXiv:1803.11190 [cond-mat.mes-hall].
 - [25] Cenke Xu and Leon Balents, “Topological superconductivity in twisted multilayer graphene,” *Phys. Rev. Lett.* **121**, 087001 (2018).
 - [26] Y.-H. Zhang, D. Mao, Y. Cao, P. Jarillo-Herrero, and T. Senthil, “Moiré Superlattice with Nearly Flat Chern Bands: Platform for (Fractional) Quantum Anomalous Hall Effects and Unconventional Superconductivity,” ArXiv e-prints (2018), arXiv:1805.08232 [cond-mat.str-el].
 - [27] Mikito Koshino, Noah F. Q. Yuan, Takashi Koretsune, Masayuki Ochi, Kazuhiko Kuroki, and Liang Fu, “Maximally localized wannier orbitals and the extended hubbard model for twisted bilayer graphene,” *Phys. Rev. X* **8**, 031087 (2018).
 - [28] Jian Kang and Oskar Vafeek, “Symmetry, maximally localized wannier states, and a low-energy model for twisted bilayer graphene narrow bands,” *Phys. Rev. X* **8**, 031088 (2018).
 - [29] Sujay Ray and Tanmoy Das, “Wannier pairs in the superconducting twisted bilayer graphene and related systems,” arXiv preprint arXiv:1804.09674 (2018).
 - [30] Francisco Guinea and Niels R Walet, “Electrostatic effects and band distortions in twisted graphene bilayers,” arXiv preprint arXiv:1806.05990 (2018).
 - [31] Biao Lian, Zhijun Wang, and B Andrei Bernevig, “Twisted bilayer graphene: A phonon driven superconductor,” arXiv preprint arXiv:1807.04382 (2018).
 - [32] Jian Kang and Oskar Vafeek, “Strong coupling phases of partially filled twisted bilayer graphene narrow bands,” arXiv e-prints , arXiv:1810.08642 (2018), arXiv:1810.08642 [cond-mat.str-el].
 - [33] Biao Lian, Fang Xie, and B. Andrei Bernevig, “The Landau Level of Fragile Topology,” arXiv e-prints , arXiv:1811.11786 (2018), arXiv:1811.11786 [cond-mat.mes-hall].
 - [34] Pablo San-Jose and Elsa Prada, “Helical networks in twisted bilayer graphene under interlayer bias,” *Phys. Rev. B* **88**, 121408 (2013).
 - [35] R. de Gail, M. O. Goerbig, F. Guinea, G. Montambaux, and A. H. Castro Neto, “Topologically protected zero modes in twisted bilayer graphene,” *Phys. Rev. B* **84**, 045436 (2011).
 - [36] Hoi Chun Po, Liujun Zou, T. Senthil, and Ashvin Vishwanath, “Faithful Tight-binding Models and Fragile Topology of Magic-angle Bilayer Graphene,” arXiv:1808.02482 [cond-mat] (2018), arXiv: 1808.02482.
 - [37] Zhida Song, Zhijun Wang, Wujun Shi, Gang Li, Chen Fang, and B Andrei Bernevig, “All” magic angles” are” stable” topological,” arXiv preprint arXiv:1807.10676 (2018).
 - [38] Junyeong Ahn, Sungjoon Park, and Bohm-Jung Yang, “Failure of nielsen-ninomiya theorem and fragile topology in two-dimensional systems with space-time inversion symmetry: application to twisted bilayer graphene at magic angle,” arXiv preprint arXiv:1808.05375 (2018).
 - [39] Liujun Zou, Hoi Chun Po, Ashvin Vishwanath, and

- T. Senthil, “Band structure of twisted bilayer graphene: Emergent symmetries, commensurate approximants, and wannier obstructions,” *Phys. Rev. B* **98**, 085435 (2018).
- [40] Jianpeng Liu, Junwei Liu, and Xi Dai, “A complete picture for the band topology in twisted bilayer graphene,” arXiv preprint arXiv:1810.03103 (2018).
- [41] Kasra Hejazi, Chunxiao Liu, Hassan Shapourian, Xiao Chen, and Leon Balents, “Multiple topological transitions in twisted bilayer graphene near the first magic angle,” arXiv preprint arXiv:1808.01568 (2018).
- [42] J. M. B. Lopes dos Santos, N. M. R. Peres, and A. H. Castro Neto, “Graphene bilayer with a twist: Electronic structure,” *Phys. Rev. Lett.* **99**, 256802 (2007).
- [43] Barry Bradlyn, L. Elcoro, Jennifer Cano, M. G. Vergniory, Zhijun Wang, C. Felser, M. I. Aroyo, and B. Andrei Bernevig, “Topological quantum chemistry,” *Nature* **547**, 298–305 (2017).
- [44] M. G. Vergniory, L. Elcoro, Zhijun Wang, Jennifer Cano, C. Felser, M. I. Aroyo, B. Andrei Bernevig, and Barry Bradlyn, “Graph theory data for topological quantum chemistry,” *Phys. Rev. E* **96**, 023310 (2017).
- [45] B Amorim and Eduardo V Castro, “Electronic spectral properties of incommensurate twisted trilayer graphene,” arXiv preprint arXiv:1807.11909 (2018).
- [46] Samuel V Gallego, Emre S Tasci, G Flor, J Manuel Perez-Mato, and Mois I Aroyo, “Magnetic symmetry in the Bilbao crystallographic server: a computer program to provide systematic absences of magnetic neutron diffraction,” *Journal of Applied Crystallography* **45**, 1236–1247 (2012).
- [47] M. G. Vergniory, L. Elcoro, C. Felser, B. A. Bernevig, and Z. Wang, “The (high quality) topological materials in the world,” arXiv preprint arXiv:1807.10271 (2018).
- [48] Tiantian Zhang, Yi Jiang, Zhida Song, He Huang, Yuqing He, Zhong Fang, Hongming Weng, and Chen Fang, “Catalogue of topological electronic materials,” arXiv preprint arXiv:1807.08756 (2018).
- [49] Feng Tang, Hoi Chun Po, Ashvin Vishwanath, and Xiangang Wan, “Towards ideal topological materials: Comprehensive database searches using symmetry indicators,” arXiv preprint arXiv:1807.09744 (2018).
- [50] See Supplemental Material with the numerical investigation of p-h symmetry breaking, more details on the symmetries and the positions of the Dirac points at $\alpha = 0$.
- [51] Y. Cao, J. Y. Luo, V. Fatemi, S. Fang, J. D. Sanchez-Yamagishi, K. Watanabe, T. Taniguchi, E. Kaxiras, and P. Jarillo-Herrero, “Superlattice-induced insulating states and valley-protected orbits in twisted bilayer graphene,” *Phys. Rev. Lett.* **117**, 116804 (2016).

Supplementary information for: Flat bands and perfect metal in trilayer moiré graphene

BREAKING PARTICLE-HOLE SYMMETRY

The particle-hole (p-h) symmetry is important in proving that all bands in the spectrum of trilayer twisted graphene are connected. It gives a band landscape symmetric with respect to zero energy and implies that features, such as Dirac points and other gapless crossings, or symmetries occurring at finite energy always come in pairs. It maintains globally the gapless structure of the spectrum. The other essential symmetry is the combined spatial-time symmetry $C_{2z}\mathcal{T}$ - this symmetry locally maintains the gapless structure of the band spectrum. Breaking $C_{2z}\mathcal{T}$ directly opens gaps at Dirac points locally and hence isolates finite sets of bands. In contrast to that, we expect the gapless band structure to keep its integrity if the terms breaking p-h symmetry are not too strong.

In a real trilayer graphene system, the rotation angles between the planes are finite and there are corrections to the emergent Eq. (1) of the main text. There are two main effects that break p-h symmetry: (i) k^2 corrections to the Dirac cones approximation $\sim \mathbf{k} \cdot \boldsymbol{\sigma}$ close to the K points in each layer, (ii) the three K points are not aligned at finite rotation angle. We note that (i) is the first step towards the complete band structure of each graphene layer with both the K and K' points. The vicinities of K and K' are indeed fully decoupled in Eq. (1) of the main text. (ii) can be simply taken into account by choosing a different basis in each layer such that the vectors \mathbf{q}_1^{ab} are parallel. This results into the Hamiltonian

$$H^{(ab)}(\delta\mathbf{p}_a, \delta\mathbf{p}_b) = v_F (M_{\theta_{1a}}^{-1} \delta\mathbf{p}) \cdot \boldsymbol{\sigma} \delta_{a,b} + w^{ab} \sum_{j=1}^3 \delta_{\delta\mathbf{p}_a, \delta\mathbf{p}_b + \mathbf{q}_j^{a,b}} T^j \quad (\text{S-11})$$

where $M_{\theta_{1a}}$ is the in-plane rotation of angle θ_{1a} , reducing to Eq. (1) of the main text for vanishingly small twist angles. Eq. (S-11) explicitly breaks p-h symmetry. The numerical resolution of Eq. (S-11) is displayed in Fig. S-3 for the representative case $p = q = 1$ and for several values of α . Inspecting the 20 states close to the Fermi energy along symmetry lines, we find band crossings between all states despite the breaking of p-h symmetry.

SYMMETRIES FOR ARBITRARY p AND q

We first review the particular case $p = q = 1$. The effective single-valley model of Eq. (1) (see main text) is obtained by keeping only the states close to the K point in each layer. It is decoupled from its time-reversed counterpart built with the states around the K' points. Hence, Eq. (1) does not respect time-reversal symmetry. For $p = q = 1$, the symmetry group of this one-valley model is the magnetic space group $P6'2'2$, the same as for twisted bilayer graphene, characterized by the generators

$$C_{3z} = \exp(i2\pi\sigma_z/3)\delta_{Q_m, C_{3z}Q_n}, \quad C_{2x} = \sigma_x \delta_{Q_m, C_{2x}Q_n}, \quad C_{2z}\mathcal{T} = \sigma_x \delta_{Q_m, Q_n} K. \quad (\text{S-12})$$

The band spectrum is invariant with respect to these three symmetries. The antiunitary $C_{2z}\mathcal{T}$ symmetry is a combination of time-reversal and C_{2z} symmetry acting locally on the moiré lattice. It commutes with the spatial symmetries C_{3z} and C_{2x} . Whereas C_{3z} maps each layer into itself, C_{2x} exchanges the layers 1 and 3 and leaves the layer 2 invariant.

Besides the magnetic space group $P6'2'2$, the model also exhibits a particle-hole (p-h) symmetry inherited from the original p-h symmetry in each graphene layer. The corresponding operator - see Eq. (7) and (8) in the main text -

$$\mathcal{P} = \delta_{Q_m, -Q_n} \zeta_{Q_n}, \quad \mathcal{P}\tilde{H}(k)\mathcal{P}^\dagger = -\tilde{H}(-k), \quad (\text{S-13})$$

commutes with the generators (S-12) of the magnetic space group, and squares to 1 in contrast with the p-h operator in the bilayer case which squares to -1 .

The rotation symmetry C_{3z} and the antiunitary symmetry $C_{2z}\mathcal{T}$ are valid also for arbitrary p and q , *i.e.* when the rotation angles are different but still commensurate. Interestingly, if p or q is different from 1, the symmetries C_{2x} and \mathcal{P} are individually broken but their product $C_{2x}\mathcal{P}$ remains a symmetry of the one-valley Hamiltonian (4) (see main text). We thus introduce the mirror p-h symmetry operator

$$\Pi_{\pi/6} = \mathcal{P}C_{2x}C_{3z} = \begin{pmatrix} 0 & e^{-2i\pi/3} \\ e^{2i\pi/3} & 0 \end{pmatrix} \delta_{Q_m, \Pi_{\pi/6}Q_n} \zeta_{Q_n}; \quad \zeta_{Q_1} = \zeta_{Q_3} = 1; \quad \zeta_{Q_2} = -1, \quad (\text{S-14})$$

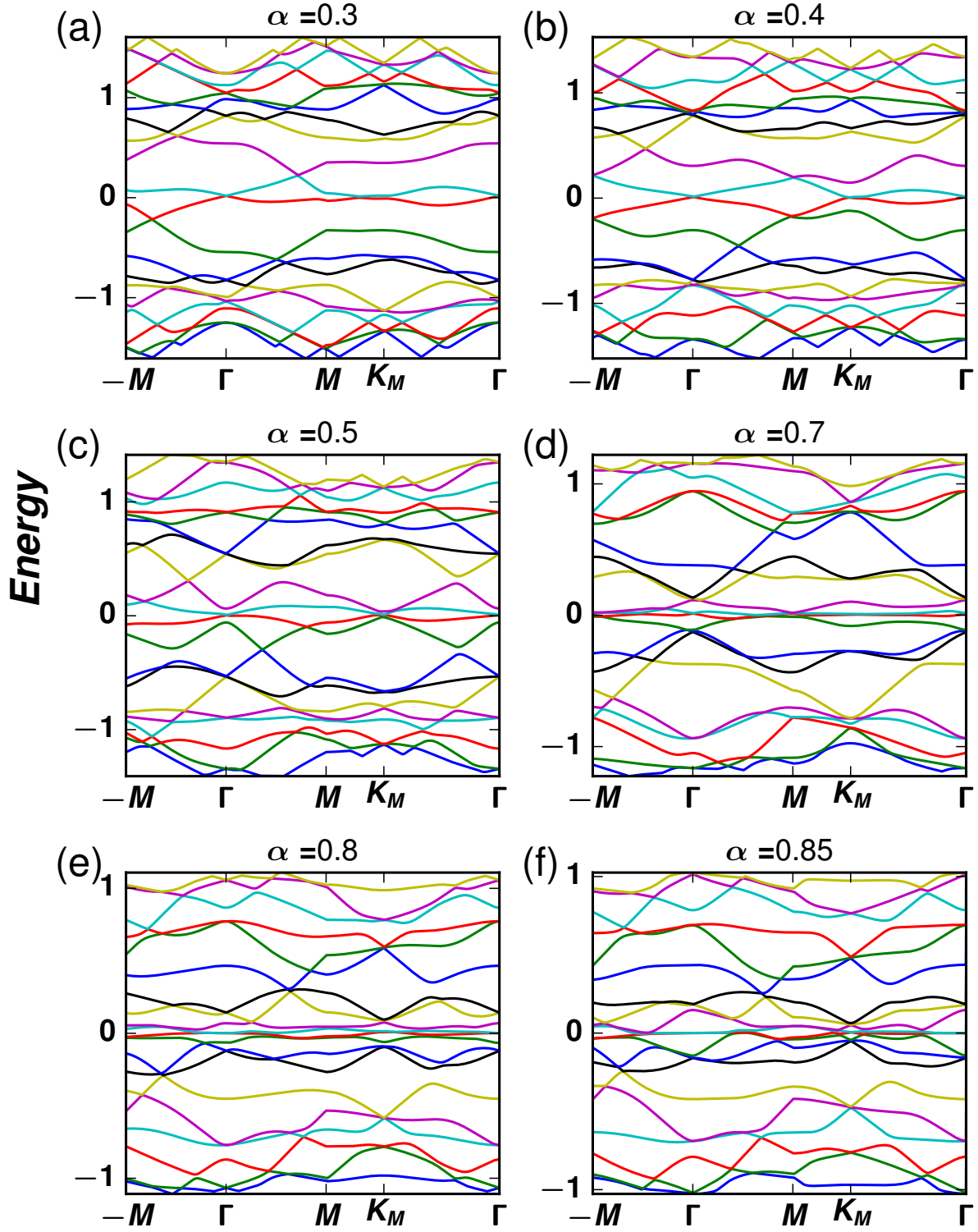


FIG. S-3. Moiré bands computed from Eq. (S-11) for $p = q = 1$ and $\theta_{1,2} = \theta_{23}$. 20 bands around zero energy are represented along the moiré Brillouin zone trajectory $-M \rightarrow \Gamma \rightarrow M \rightarrow K_M \rightarrow \Gamma$ for $\alpha = 0.3, 0.4, 0.5, 0.7, 0.8, 0.85$ (a-f). In principle, Eq. (S-11) has two independent parameters, α and θ_{12} , and the ratio between them is not universal. For this plot, we have nevertheless chosen the conversion rule $\theta_{12} = 1.05^\circ$ for $\alpha = 0.606$ compatible with experiment results on graphene structures.

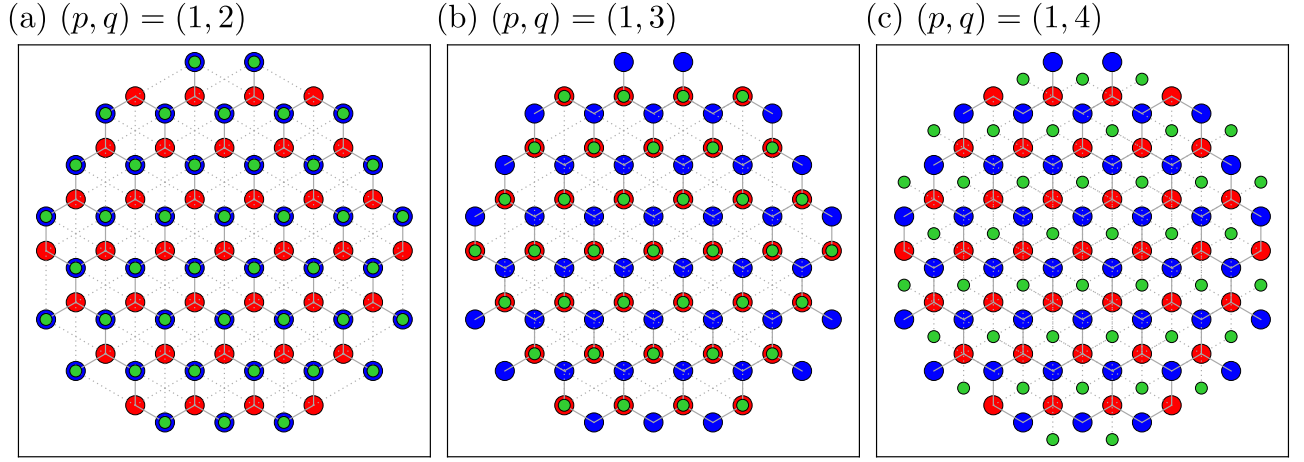


FIG. S-4. Three lattices of Dirac cones for $\alpha = 0$ corresponding to different $(p, q) = (1, 2)$ (a), $(1, 3)$ (b), and $(1, 4)$ (c). Red (resp. blue, green) points correspond to the middle (resp. bottom, top) layer. The right lattice (c) has separate Dirac cones, corresponding to the case (i) (see supplementary main text), whereas the left (a) and middle (b) lattices have pairs of overlapping Dirac cones and 1 isolated Dirac cone, corresponding to the case (ii) of the supplementary main text.

obtained by combining the product $\mathcal{C}_{2x}\mathcal{P}$ with the rotation symmetry \mathcal{C}_{3z} . ζ_{Q_n} is $+1$ for Q_n belonging to the bottom and top layers and -1 for the middle layer. The invariant plane of the mirror symmetry $\Pi_{\pi/6}$ crosses orthogonally the graphene layers along lines. These lines make an angle of $\pi/6$ with respect to the x axis and go through the Γ and K_M points. By construction, each layer is thus invariant upon the mirror symmetry $\Pi_{\pi/6}$. The action on the Hamiltonian (4) is

$$\Pi_{\pi/6}\tilde{H}(k)\Pi_{\pi/6}^\dagger = -\tilde{H}(\Pi_{\pi/6}k), \quad (\text{S-15})$$

corresponding to a p-h symmetry. Eq. (S-15) implies a symmetric band spectrum around zero energy where each state k has a mirror-symmetric partner $\Pi_{\pi/6}k$ with opposite energy.

POSITIONS OF THE DIRAC CONES FOR $\alpha = 0$

As discussed in the main text, the full connectivity of the moiré band model requires essentially the $C_{2z}T$ symmetry to protect Dirac cones, or at least to have them gapped by pairs, the mirror p-h symmetry $\Pi_{\pi/6}$ to reduce the parity of Dirac points to their parity in the zero energy manifold, and the continuity with respect to the case $\alpha = 0$ where the positions of Dirac points are easily determined. As illustrated in Fig. S-4, we find two configurations at $\alpha = 0$: either (i) the model has three Dirac points at distinct positions Γ, K_M, K'_M in the Brillouin zone, or (ii) two Dirac points are on top of each other and separated from the third one. The case (i) occurs for $q - p = 1 \pmod 3$ whereas (ii) occurs for $q - p = 0, 2 \pmod 3$.

DENSITIES OF ELECTRONS CLOSE TO THE FERMI ENERGY

Twisted bilayer graphene, with a small angle, exhibits a local density of states for the (almost) flat bands that is well-localized to the AA regions of the Moiré pattern [4, 7, 51], forming a triangular lattice. This spatial localization is understood at zero energy from the absence of tunneling between AA and AB, BA regions [6]. In the trilayer geometry, it is not possible to isolate a finite set of bands as we prove in the main text. However, we can integrate the local density of states (LDOS) over a narrow energy range close to zero energy similarly to what has been done in the bilayer case [6]. The result is shown in Fig. S-5 for $\alpha = 0.28, 0.42, 0.85$. In the middle layer, localization around the AA region occurs more dramatically when bands are nearly dispersionless close, see $\alpha = 0.85$. Although the whole pattern forms a triangular lattice, the localization around the AA region is never really strong for the lower and top layers.

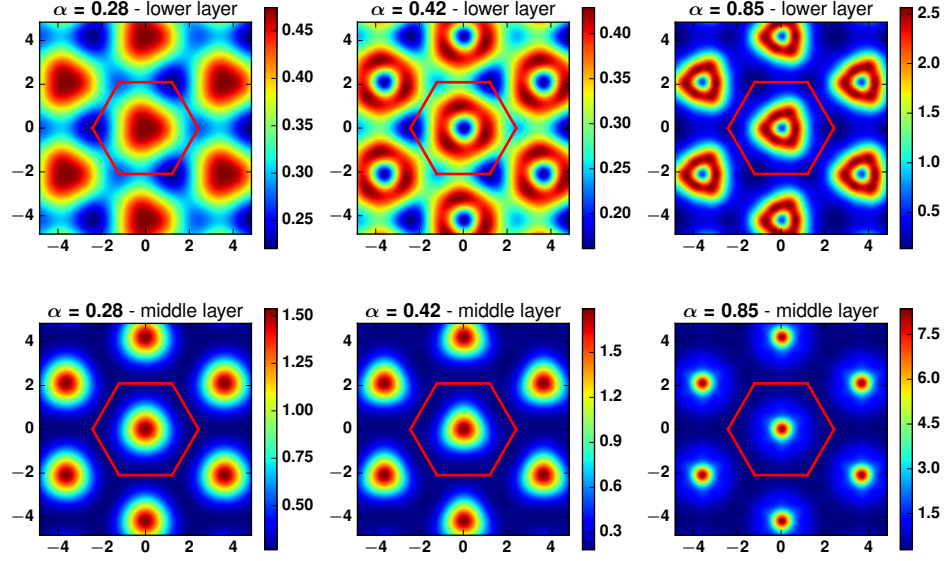


FIG. S-5. Local density of states for the A sublattice, and $p = q = 1$, integrated for $|\varepsilon| < \varepsilon_{\max}$. Its counterpart for the B sublattice is inferred by C_6 symmetry, and the upper layer one is obtained from the lower layer by particle-hole symmetry. We choose $\varepsilon_{\max} = 0.02$ and $\alpha = 0.28, 0.42, 0.85$.